Pharmaceutical Research, Vol. 23, No. 4, April 2006 (© 2006)
DOI: 10.1007/s11095-006-9662-5

Research Paper

Long Circulating Poly(Ethylene Glycol)-Decorated Lipid Nanocapsules Deliver Docetaxel to Solid Tumors

Mohamed Nabil Khalid,[1] Pierre Simard,[1] Didier Hoarau,[2] Alice Dragomir,[1] and Jean-Christophe Leroux[1,3]

Received June 10, 2005; accepted December 6, 2005

Purpose. The purpose of this study was to evaluate the ability of poly(ethylene glycol)-coated lipid nanocapsules (LN) to deliver the highly potent hydrophobic anticancer drug docetaxel to solid tumors.
Methods. Docetaxel-loaded nanocapsules (80–120 nm) were produced by a solvent-free phase inversion process and were coated with polyethylene glycol distearoylphosphatidylethanolamine conjugate by a postinsertion step. *In vivo* studies were conducted in mice bearing subcutaneously implanted C26 colon adenocarcinoma to assess the pharmacokinetics and biodistribution of both the drug and LN.
Results. Incorporation of docetaxel into the LN dramatically increased the drug's biological half-life while providing substantial accumulation at the tumoral site. The pharmacokinetics and biodistribution pattern were found to depend on the specific surface area and shell composition of the nanocapsules.
Conclusion. This study demonstrates that docetaxel physically entrapped into a lipid colloidal drug carrier can be efficiently targeted to neoplastic tissues.

KEY WORDS: docetaxel; drug targeting; nanocapsules; pharmacokinetics; poly(ethylene glycol).

INTRODUCTION

Nanoscopic drug carrier systems, such as liposomes (1), nanoparticles (2), and polymeric micelles (3), can change the biodistribution of active substances and increase their therapeutic index. However, the potential and applicability of such systems in the pharmaceutical field are closely related to their physicochemical properties and their interactions with the host. After intravenous (i.v.) injection, colloidal drug carriers are generally recognized as foreign bodies and are thus rapidly cleared from the systemic circulation by the mononuclear phagocyte system (MPS), mainly the Kupffer cells of the liver and macrophages of the spleen (4). A widely used and effective method to slow down clearance by the immune system is to incorporate poly(ethylene gycol) (PEG) derivatives at the colloid surface. Because of its hydrophilicity and flexibility, PEG creates a zone of steric hindrance around the carrier, which decreases its rate of uptake by the MPS and prolongs its biological half-life. PEGylation has been successfully applied to liposomes (5,6) and nanoparticles (7), especially in the field of cancer chemotherapy. Indeed, by increasing the residence time of an antineoplastic drug in the central compartment, its redirection to tumoral sites becomes possible (1,8). Unlike most healthy tissues, tumors possess a leaky vasculature that allows the passage of colloidal particles in the range of 50–200 nm (9–11). Moreover, lymphatic drainage is generally impaired in the tumoral interstitium, favoring retention of the carrier and its transported cargo at the extravasation site. This characteristic is often referred to as the enhanced permeation and retention (EPR) effect (10). Although the EPR effect has been exploited for the selective tumor delivery of a number of cytotoxic agents, most attempts aimed at targeting taxanes, one of the most important classes of anticancer drugs discovered over the past decades, have met with moderate success (12–16). Taxanes are microtubule inhibitors that display substantial antitumor efficacy against breast, ovarian, prostate, and nonsmall cell lung cancer. To date, two taxanes, namely, paclitaxel (PTX) and docetaxel (DTX), have been introduced on the market. Although PTX is still the most widely used taxane, DTX is more potent in terms of promotion of tubulin polymerization, inhibition of depolymerization and of cell replication, as well as antitumor activity in many *in vitro* and *in vivo* models (17,18). Despite their strong anticancer activity, taxanes exhibit serious dose-limiting toxicities and hypersensitivity reactions, which come from the formulating vehicles and the absence of selectivity for target tissues (19–21). Both drugs are poorly water-soluble and are formulated as micellar solutions of low-molecular-weight surfactants, namely, cremophor EL and polysorbate 80 for PTX and DTX, respectively. Approaches aimed at reformulating taxanes with colloidal carriers have, in most cases, resulted in better tolerance to treatment (use of safer excipients) without, however, altering the drug biodistribution patterns or improving their tumor localization (12,15,22). These rather disappointing findings have been mainly attributed to the rapid and complete release of

[1] Canada Research Chair in Drug Delivery, Faculty of Pharmacy, University of Montreal, C.P. 6128 Succ, Centre-ville, Montreal (QC) H3C 3J7, Canada.
[2] Ethypharm Inc., 200 boul. Armand Frappier, Laval (QC) H7V4A6, Canada.
[3] To whom correspondence should be addressed. (e-mail: Jean-Christophe.Leroux@umontreal.ca)

encapsulated taxanes from the carrier into the bloodstream upon their introduction in the systemic circulation (23). Several strategies are currently being assessed to minimize leakage by introducing chemical (24) or physical (22) cross-links into nanocarriers or by enhancing compatibility between the drug and vector (25). However, despite some success with recent vehicles (26–28), there is still an unmet clinical need to develop safe and targeted drug delivery strategies for taxanes. The purpose of this study was to evaluate the ability of lipid nanocapsules (LN) to deliver DTX to solid tumors. The LN were coated with a PEG lipid to maximize the biological half-life of the carrier (29) and drug, and their subsequent deposition in tumoral tissues.

MATERIALS AND METHODS

Materials

PEG 660 12-hydroxystearate (PEG-HS, Solutol® HS15) was a kind gift from BASF (Ludwigshafen, Germany). Hydrogenated soybean phosphatidylcholine (HSPC, >99% phosphatidylcholine) and 1,2-distearoyl-*sn*-glycero-3-phosphatidylethanolamine-*N*-monomethoxy–[PEG 2000] (DSPE–PEG) were purchased from Northern Lipids Inc. (Vancouver, BC, Canada). Tricaprylin, [^{3}H]cholesteryl hexadecyl ether ([^{3}H]CHE), Sephadex® G50, and Sepharose® CL-4B were obtained from Sigma-Aldrich (Oakville, ON, Canada) and Perkin Elmer (Woodbridge, ON, Canada). Bulk DTX was supplied by the Shanghai Fudan Taxusal New Technology Co. (Shanghai, China), respectively. The control DTX formulation (Taxotere®, TXT, Aventis Pharma Ltd., Dagenham, UK) was purchased in a retail pharmacy. All products were used without further purification. Hionic-Fluor® [1,2,4-trimethylbenzene, 40–60%; bis(2-ethylhexyl) hydrogen phosphate, 10–20%; ethoxylated alkylphenol, 10–20%; triethyl phosphate, 2.5–10%; sodium docusate, 2.5–10%; 2,5-diphenyloxazole, <2.5%; 1,4-bis-(4-methyl-alpha-styryl)-benzene, <2.5%] and Soluene 350® were obtained from Perkin Elmer and Camberra Packard (Mississauga, ON, Canada), respectively. Water was deionized with a Milli-Q® purification system (Millipore, Bedford, MA, USA) before use.

Preparation and Characterization of Nanocapsules

LN were prepared by a phase inversion-based process, as described previously (30). Briefly, the constituents of the shell, viz. PEG-HS and HSPC, of the core, viz. tricaprylin and DTX (3% *w/w* of total LN constituents), and of the dispersing phase (~4.4% *w/v* NaCl in water), were combined to obtain a total mass of 5 g. The lipid phase typically represented 17–22% of the emulsion mass. The different components were mixed under magnetic stirring and heated above the phase transition temperature (ca. 85°C). The mixture was cooled down to 60°C to produce an *o/w* nanoemulsion and then reheated above the phase inversion zone to give a *w/o* system. This cycle was repeated three times, and the *o/w* emulsion was quenched by the addition of 12.5 mL water at 4°C. PEGylated LN (P-LN) were prepared by incubating preformed LN at 60°C for 90 min with DSPE–PEG (15 mg mL^{-1}) at varying concentrations (6, 10, and 15 mol% of total shell components), as previously described (29). The mean hydrodynamic diameter of the LN was assessed at 25°C by dynamic light scattering with a Coulter N4Plus (Coulter Electronics, Miami, FL, USA) at a fixed angle of 90°. Measurements were performed in triplicate after dilution of the suspension in water.

The drug loading efficiency was determined using LN that were doped with the nonexchangeable lipid marker [^{3}H]CHE and [^{14}C]DTX to track the vector and drug, respectively. Free DTX was separated from encapsulated DTX by gel filtration over a Sephadex® G50 column (1× 30 cm). The radioactivity of collected fractions was measured in a scintillation counter (Liquid Scintillation Analyser Tri-Carb 2100TR; Packard, Meriden, CT, USA) after the addition of Hionic Fluor® scintillation cocktail. The *in vitro* release of DTX was also assessed after the incubation of radiolabeled LN in a saline solution (0.9% NaCl *w/v*) containing 40 mg mL^{-1} bovine serum albumin at 37°C for 2 h. Released DTX was separated from LN by size exclusion chromatography on a Sepharose® CL-4B column (1×30 cm) and assayed as described above. The albumin content in each fraction was measured using the BCA protein assay kit (Pierce, Rockford, IL, USA).

Pharmacokinetic and Biodistribution Studies

For the pharmacokinetic and biodistribution studies, radiolabeled DTX-loaded LN formulations were prepared as described above and diluted with NaCl 0.9% (*w/v*) to adjust the drug dose for injection. *In vivo* experiments were performed on female Balb/C mice (18–21 g) inoculated with C26 colon adenocarcinoma cells, following a protocol approved by the Animal Welfare and Ethics Committee of the University of Montreal in accordance with Canadian Council on Animal Care guidelines. One day before tumor implantation, hair on the hind legs and back of the mice was removed by shaving. C26 cells were harvested by trypsinization and resuspended in growth medium. Approximately 2×10^6 cells in 50 μL growth medium was injected subcutaneously in three different locations on the back of each mouse, which produced three separate tumors. The formulations were administered 10 days after cell inoculation, when each tumor grew to a volume of approximately 20 mm^3. Tumor volume was calculated as $1/2(4\pi/3)(L/2)(W/2)H$, where L is the length, W is the width, and H is the height of the tumor. Tumor-bearing mice were anesthetized with isoflurane, and injected *via* the subclavian vein with TXT, LN-DTX, or P-LN-DTX at 1 and 15 mg kg^{-1} for a total volume of 8 μL g^{-1} of body weight. Each mouse received 0.8 and 0.3 μCi of [^{3}H]CHE and [^{14}C]DTX, respectively.

At different time points after drug administration, the mice (n = 4–5 per experimental group) were sacrificed. The biological variation due to sampling time was less than 25%. Blood was sampled by cardiac puncture, and organs/tissues of interest (liver, spleen, kidneys, and tumor) were harvested for drug and LN content analysis. Blood and tissues were weighed and treated with isopropanol/Soluene 350®. After digestion, the blood samples were bleached by successive additions of hydrogen peroxide (H_2O_2, 30% *v/v*). The samples were left to stand in the dark overnight at 4°C following the addition of Hionic Fluor® scintillation cocktail.

Table I. Nanocapsule Formulations Administered to C26 Tumor-Bearing Mice

Formulation	Tricaprylin (% w/w)	PEG-HS (% w/w)	HSPC (% w/w)	PEG-DSPE (mol%)[b]	Diameter ± SD (nm)
TXT[a]	–	–	–	–	–
LN	51.5	40.8	7.7	–	70 ± 10
P-LN-6-80	51.5	40.8	7.7	6	80 ± 8
P-LN-10-80	51.5	40.8	7.7	10	80 ± 8
P-LN-6-120	54.2	37.7	8.1	6	117 ± 12
P-LN-10-120	54.2	37.7	8.1	10	118 ± 10
P-LN-15-120	54.2	37.7	8.1	15	118 ± 10

[a] DTX in polysorbate 80 at a concentration of 40 mg mL^{-1}.
[b] Expressed as mol% of total surface components (excluding tricaprylin).

Radioactivity was then measured using the scintillation counter in dual mode ($^3H/^{14}C$). The scintillation counter provides radioactivity counts that are corrected according to a quench curve established for biological samples. These counts were converted to a concentration using the total amount of injected dose and its associated counts. The mean area under the blood concentration *vs.* time curve (AUC), blood clearance (CL), and other pharmacokinetic parameters were determined using a noncompartmental model with PK Solutions 2.0 software (Summit Research Services, Montrose, CO, USA). Differences between AUC group means were analyzed by the two-tailed *t* test for independent samples. AUCs were calculated using resample bootstrap methods with 1,000 simulations (S-plus 2000 Professional for Windows; MathSoft, Inc., Cambridge, MA, USA). To compare the formulations at each time point, a one-way analysis of variance with Tukey's post-hoc test for multiple comparisons was performed using SPSS 11.0 software (SPSS Inc., Chicago, IL, USA). $p < 0.01$ was the level of significance.

RESULTS AND DISCUSSION

LN with sizes ranging from 80 to 120 nm and low polydispersities (<0.2) were prepared by adjusting the phospholipid/surfactant to tricaprylin ratio. Postinsertion of DSPE–PEG was associated with an ~10 nm increase in nanocapsule diameter (Table I). This size increment corresponds approximately to twice the thickness of a PEG 2000 coating in brush conformation (31). Incorporation of 3% (*w/w*) DTX did not impact the size of the LN. Entrapment efficiency was evaluated after separating the free from the encapsulated drug by size exclusion chromatography. It was found to be superior to 98% (Fig. 1A). Two hours after incubation in a saline solution containing a physiological concentration of albumin, uncoated LN (120 nm) were shown to release 76% of entrapped DTX (Fig. 1B), indicating rapid drug exchange with serum protein. The PEG coating (formulation P-LN-15-120 in Table I) decreased the leakage to 57% (Fig. 1C), possibly by preventing proteins from interacting with the lipid surface (32). Accordingly, several DTX-loaded LN differing in PEG content (6, 10, and 15 mol%) and size (80 and 120 nm) were prepared and evaluated *in vivo* (Table I).

Blood concentrations of nanocapsules and DTX after i.v. injection of formulated drug at 1 mg kg^{-1} to mice bearing s.c. implanted C26 adenocarcinoma are depicted in Fig. 2A and B, respectively. Non-PEGylated LN (80 nm) were rapidly cleared from the systemic circulation, with less than 10% of the injected dose remaining in blood 2 h postinjection (Fig. 2A). Indeed, as previously observed in the rat model (29), uncoated LN were avidly taken up by the liver and less by the spleen (75 *vs.* 15%/g, respectively, after 12 h). As shown in Fig. 2B, the corresponding drug levels in blood were even

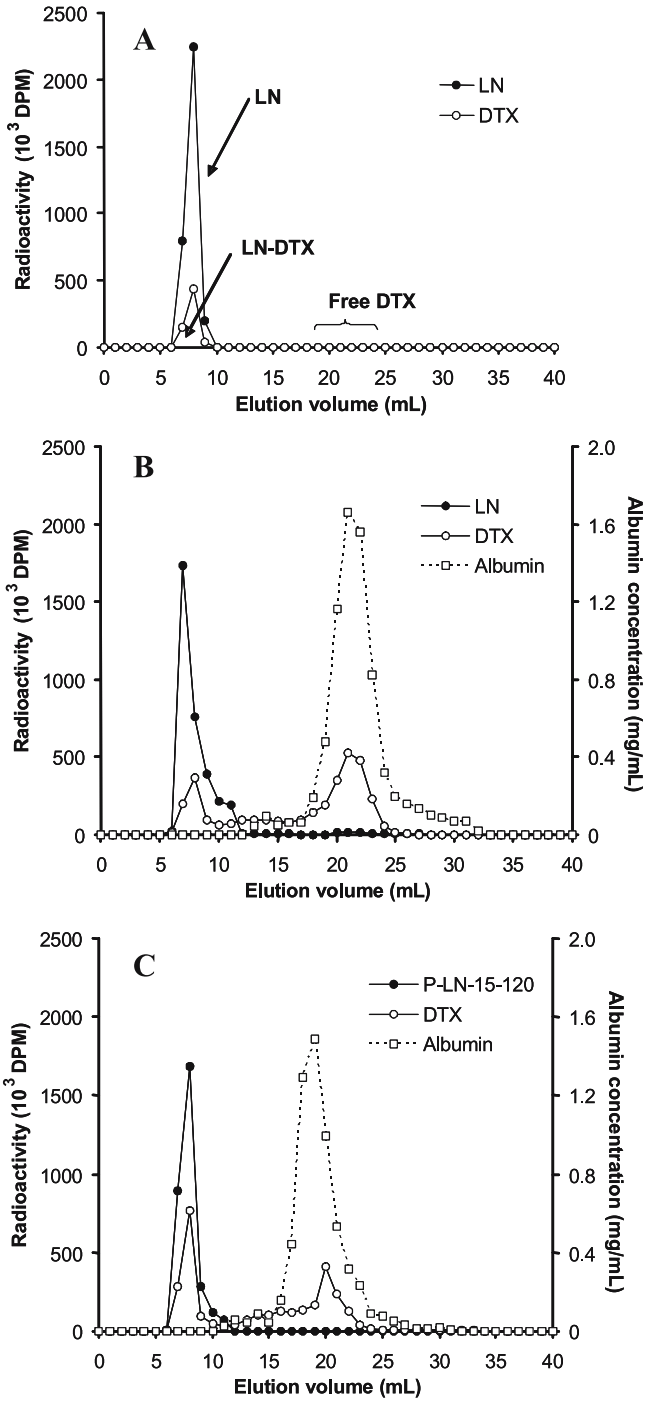

Fig. 1. Elution profile of LN and encapsulated DTX (LN–DTX) after preparation (A). Elution profiles of DTX-loaded LN (B) and P-LN-15-120 (C) after incubation in a saline solution containing 40 mg mL^{-1} albumin for 2 h at 37°C. The nanocapsules were labeled with 2×10^{-2} μCi mg^{-1} [^{3}H]CHE and initially loaded with 3% (*w/w*) DTX spiked with 0.5×10^{-2} μCi mg^{-1} [^{14}C]DTX.

lower, reflecting both the rapid LN clearance and DTX leakage from the carrier. Two hours after administration, the DTX blood concentration of the control TXT formulation was higher than that of uncoated LN (10 *vs.* 4% of the injected dose, respectively).

PEGylation of LN at 6, 10, and 15 mol% greatly enhanced LN circulation time. All three PEGylation densities provided LN with similar blood levels after 2, 6, and 12 h (Fig. 2A) and comparable uptake by the liver and spleen (40–50%/g after 12 h). Interestingly, particle size did not influence P-LN removal from the bloodstream, as 80- and 120-nm nanocapsules PEGylated at either 6 or 10 mol% exhibited similar circulation times. In contrast, size and PEG density dramatically influenced the extent of drug release from the nanocapsules. For particles of 80 nm, increasing PEG content from 6 to 10 mol% gave an ~3-fold elevation of DTX blood levels 2 and 6 h after injection (Fig. 2B). Similarly, at a fixed PEG content of 6 mol%, augmenting particle size from 80 to 120 nm, produced a comparable effect. Two hours postinjection, the highest blood concentrations of DTX were obtained with 120 nm P-LN containing 15 mol% PEG (P-LN-15-120). From these results, it can be seen that drug leakage could be controlled by changing the physicochemical characteristics of P-LN. Although enhancing PEG density may reduce interactions and drug exchange with blood components (Fig. 1C), increasing the particle size decreases the specific surface area available for diffusion.

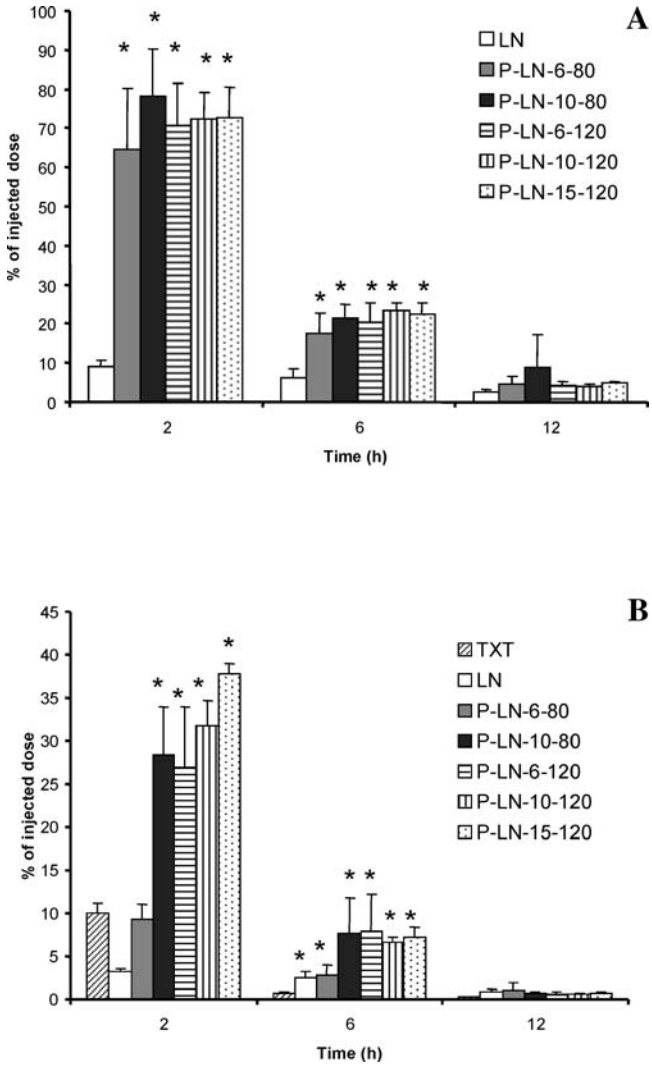

Fig. 2. Blood concentration–time profiles of nanocapsules (A) and DTX (B) after i.v. injection of various DTX formulations in mice, at a drug dose level of 1 mg kg^{-1}. Nanocapsules were loaded with 3% (*w/w*) DTX. Mean ± SD (n = 5 mice/group). Only statistically significant differences between LN and P-LN (A) or between TXT and encapsulated DTX (B) are indicated. *$p < 0.01$.

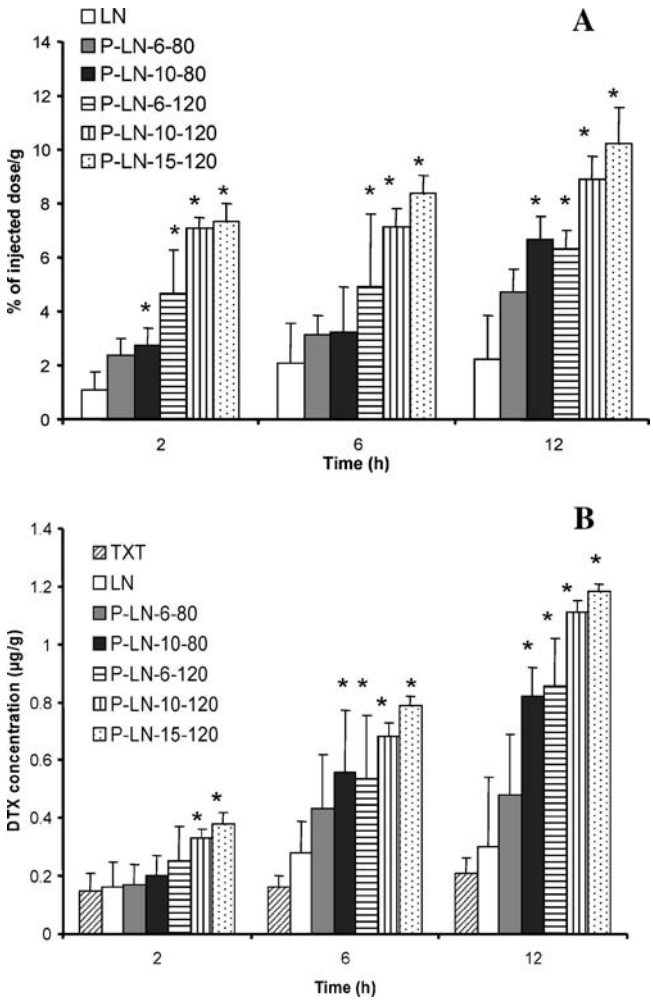

Fig. 3. Tumor concentration–time profiles of nanocapsules (A) and DTX (B) after i.v. injection of various DTX formulations in mice, at a drug dose level of 1 mg kg^{-1}. Nanocapsules were loaded with 3% (*w/w*) DTX. Mean ± SD (n = 5 mice/group). Only statistically significant differences between LN and P-LN (A) or between TXT and encapsulated DTX (B) are indicated. *$p < 0.01$.

The tumoral concentrations of both nanocapsules and DTX were monitored in parallel and are presented in Fig. 3A and B, respectively. As expected, uncoated LN accumulated poorly in C26 xenografts. The control TXT-DTX and LN-DTX mean concentrations in neoplastic tissue did not exceed 0.2–0.3 µg g^{-1}. Tumoral localization of P-LN seemed to increase with PEG density, although statistical significance could be demonstrated only between formulations containing 6 and 15 mol% of PEG at the 12-h time point. Surprisingly, 120-nm particles also seemed to accumulate slightly more in the tumors than their 80-nm counterparts (P-LN-10-120 *vs.* P-LN-10-80 at 6 and 12 h, $p < 0.01$) despite apparently similar

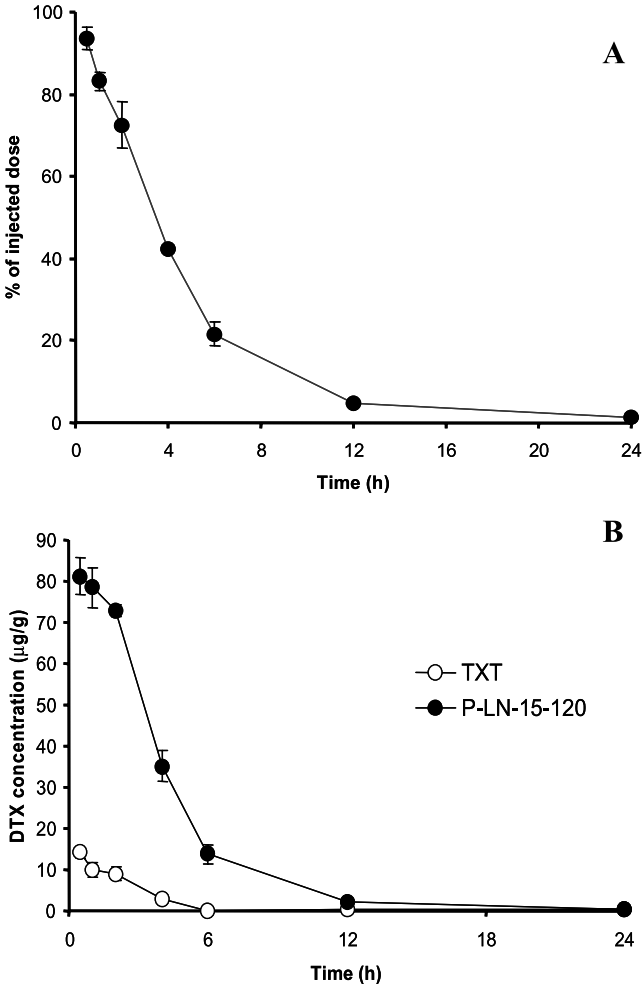

Fig. 4. Blood concentration–time profiles of nanocapsules (A) and DTX (B) after i.v. injection of TXT (open circles) or P-LN-15-120 (closed circles) in mice, at a drug dose level of 15 mg kg^{-1}. Nanocapsules were loaded with 3% (*w/w*) DTX. Mean ± SD (n = 4 mice/group).

blood profiles. Several hypotheses could explain the effect of size and PEG density on the tumoral levels of nanocapsules. First, in the case of liposomes, it has been demonstrated that the tumoral permeability coefficient of the tumor vasculature (11) as well as tissue penetration (33) increased when the vesicles were sterically shielded. Second, the difference observed in P-LN tumor levels may result from slight differences in the stability of extravasated nanocapsules in the tumoral interstitium. Some tumor tissues overexpress secretory enzymes, for example, phospholipase A_2 (34). Such enzymes could degrade the extravasated nanocapsules at a rate that may depend on particle size and PEG density in the P-LN shell. Third, the clearance of extravasated P-LN from the interstitium by the lymphatic system may also be size-dependent. Trubetskoy and Torchilin (35) have indeed demonstrated that the lymphatic uptake of colloids was inversely related to particle size.

The most significant findings of our work were that P-LN allowed DTX to accumulate substantially in C26 xenografts. Tumoral drug concentrations increased over the 12-h sampling period and largely exceeded that of the control TXT formulation (Fig. 3B) ($p < 0.01$ for P-LN-10-80, P-LN-6-120, P-LN-10-120, and P-LN-15-120 *vs.* TXT at 6 and 12 h). The highest tumoral levels were reached with P-LN-15-120, which peaked at 1.2 μg g^{-1} at 12 h. Accumulation of DTX in the tumors could be attributed to preferential P-LN deposition in the neoplastic tissue and reduced drug leakage from the formulations. In view of these promising results, a complete pharmacokinetic and biodistribution study comparing TXT and P-LN-15-120 was performed at 15 mg kg^{-1}, a dose commonly used in efficacy studies (Figs. 4, 5, and 6), and the pharmacokinetic parameters of both formulations were calculated (Table II). The PEGylated nanocapsules exhibited a long circulation time (Fig. 4A) and extravasated in the tumor (Fig. 5A). As expected, the MPS organs were the major accumulation sites for the P-LN (Fig. 5B). The liver levels peaked at 4 h (30% of injected dose g^{-1}), whereas concentrations in the spleen kept increasing up to 24 h (60% of injected dose g^{-1}). As shown in Fig. 5B, P-LN deposition in the kidneys remained low, reflecting the fact that nanoparticulate colloids within this size range (80–120 nm) are not eliminated by glomerular filtration.

The *in vivo* properties of P-LN translated into a modified pharmacokinetic profile for DTX (Table II, Fig. 4B). After bolus injection, the apparent volume of distribution (V_d) decreased from 7.2 to 1.8 L kg^{-1}, reflecting better confinement of P-LN in blood in the early phase. The biological

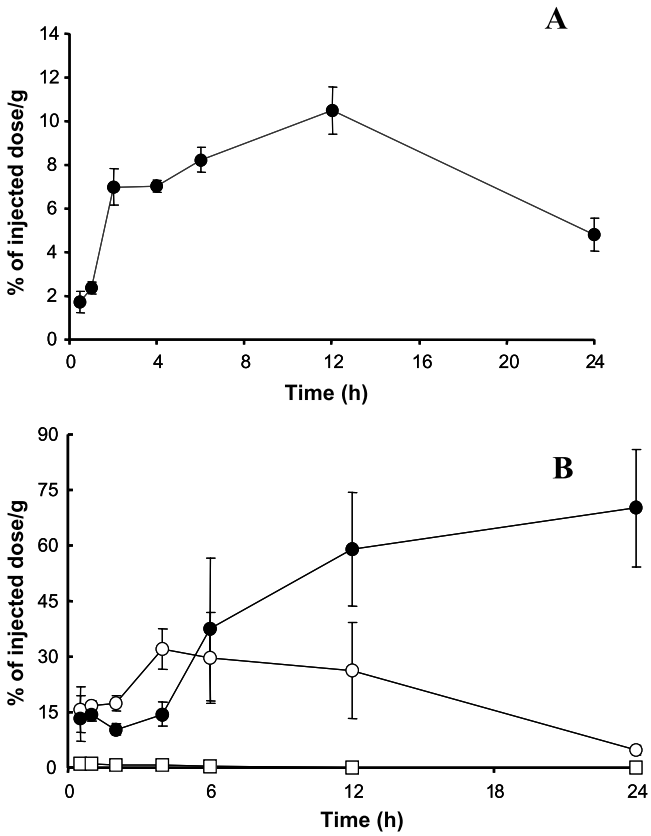

Fig. 5. Tumor (A), liver (open circles), spleen (closed circles), and kidneys (open squares) (B) concentration–time profiles of nanocapsules after i.v. injection of P-LN-15-120 in mice, at a dose of 15 mg kg^{-1}. Nanocapsules were loaded with 3% (*w/w*) DTX. Mean ± SD (n = 4 mice/group).

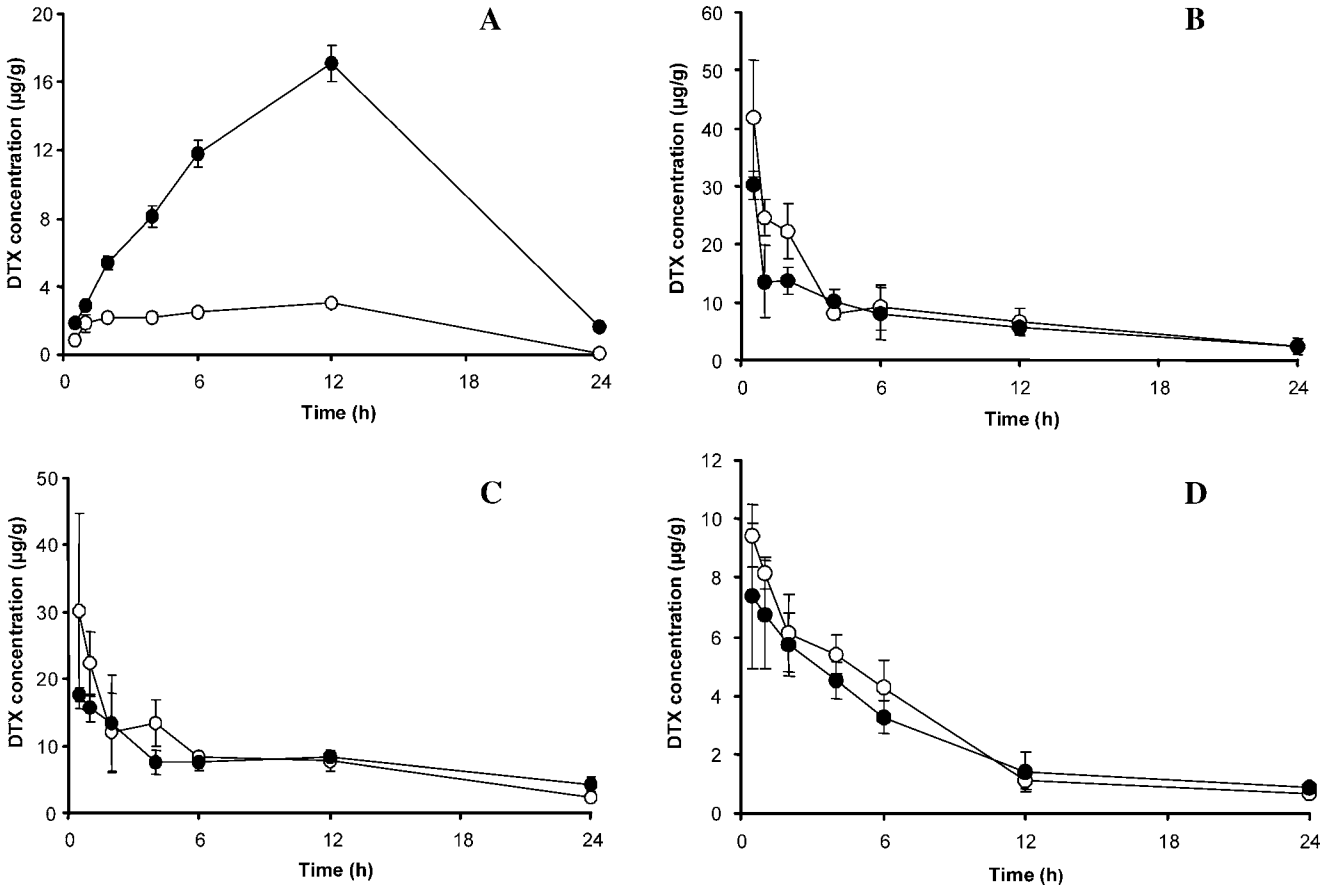

Fig. 6. Tumor (A), liver (B), spleen (C), and kidney (D) concentration–time profiles of DTX after i.v. injection of TXT (open circles) or P-LN-15-120 (closed circles) in mice, at a drug dose level of 15 mg kg^{-1}. Nanocapsules were loaded with 3% (w/w) DTX. Mean ± SD ($n = 4$ mice/group).

half-life ($t_{1/2}$), very short for the free drug (0.3 h), increased to 1.4 h for DTX entrapped in P-LN-15-120. The reduction of V_d and increment of $t_{1/2}$ resulted in a marked decrease in CL. These changes in the pharmacokinetic parameters were accompanied by a substantial deposition of drug in the tumors, which was characterized by a 5-fold increase in AUC_{tumor} compared to TXT (16.1 *vs.* 3.2 µg h g^{-1}) (Fig. 6A, Table II). With respect to the distribution in the liver, spleen, and kidneys (Fig. 6B–D), the PEGylated LN provided lower drug levels in these organs than TXT at the early time points (≤2 h). This altered biodistribution profile may eventually result in a lower drug toxicity for healthy tissues.

To the best of our knowledge, this is the first report demonstrating that DTX physically entrapped in a colloidal drug carrier could be targeted to neoplastic tissues. Comparable success has been previously achieved with PTX with macromolecular carriers such as poly(L-glutamic acid) (28). However, such an approach is more complex because it requires chemical derivatization of the drug for covalent coupling with the polymer and the hydrolysis of linkage at the target site to release PTX. Recently, Hamaguchi *et al.* (26) showed that the pharmacokinetics, biodistribution, and *in vivo* efficacy of PTX could be improved by its incorporation into tailor-made polymeric micelles prepared with a block copolymer of PEG and poly(aspartate) esterified with 4-pheny-1-butanol. Although these preliminary results are encouraging, the toxicity of this novel polymer will have to be carefully examined as the latter is not approved for parenteral administration.

Future work on LN will aim at determining the maximum tolerated dose, toxicity profile, and efficacy of DTX entrapped in P-LN in appropriate tumor models.

Table II. Mean Pharmacokinetic Parameters of TXT and P-LN-15-120 and Tumoral DTX Accumulation After Bolus i.v., Administration to Tumor-Bearing Mice

Formulation	Dose (mg kg^{-1})	$AUC_{0-24\ h}$ ± SD (µg h mL^{-1})	CL (L h^{-1} kg^{-1})	$t_{1/2}$ (h)	MRT[a] (h)	V_d (L kg^{-1})	AUC_{tumor} ± SD (µg h g^{-1})
DTX in TXT	15	7.2 ± 0.2	2.1	0.3	1.2	7.2	3.2 ± 0.1
DTX in P-LN	15	29.1 ± 0.7*	0.6	1.4	2.8	1.8	16.1 ± 0.3*
P-LN	446	39.6 ± 0.8	0.01	1.9	3.6	0.05	–

[a] Mean residence time.
*$p < 0.01$ *vs.* TXT.

ACKNOWLEDGMENT

The Canada Research Chair program is acknowledged for financial support.

REFERENCES

1. D. C. Drummond, O. Meyer, K. Hong, D. B. Kirpotin, and D. Papahadjopoulos. Optimizing liposomes for delivery of chemotherapeutic agents to solid tumors. *Pharmacol. Rev.* **51**:691–743 (1999).
2. I. Brigger, C. Dubernet, and P. Couvreur. Nanoparticles in cancer therapy and diagnosis. *Adv. Drug Deliv. Rev.* **54**:631–651 (2002).
3. M. C. Jones and J. C. Leroux. Polymeric micelles—a new generation of colloidal drug carriers. *Eur. J. Pharm. Biopharm.* **48**:101–111 (1999).
4. S. M. Moghimi, A. C. Hunt, and J. C. Murray. Long-circulating and target-specific nanoparticles: theory to practice. *Pharmacol. Rev.* **53**:283–318 (2001).
5. D. Papahadjopoulos, T. M. Allen, A. Gabizon, E. Mayhew, K. Matthay, S. K. Huang, K. D. Lee, M. C. Woodle, D. D. Lasic, C. Redemann, and F. J. Martin. Sterically stabilized liposomes: improvement in pharmacokinetics and antitumor therapeutic efficacy. *Proc. Natl. Acad. Sci. U.S.A.* **88**:11460–11464 (1991).
6. M. S. Webb, D. Saxon, F. M. P. Wong, H. J. Lim, Z. Wang, M. B. Bally, L. S. L. Choi, P. R. Cullis, and L. D. Mayer. Comparison of different hydrophobic anchors conjugated to poly(ethylene glycol): effects on the pharmacokinetics of liposomal vincristine. *Biochim. Biophys. Acta* **1372**:272–282 (1998).
7. R. Gref, Y. Minamitake, M. T. Peracchia, V. S. Trubetskoy, V. Torchilin, and R. Langer. Biodegradable long circulating polymeric nanospheres. *Science* **263**:1600–1603 (1994).
8. R. Duncan, S. Gac-Breton, R. Keane, R. Musila, Y. N. Sat, R. Satchi, and F. Searle. Polymer–drug conjugates, PDEPT and PELT: basic principles for design and transfer from the laboratory to the clinic. *J. Control. Release* **74**:135–146 (2001).
9. F. Yuan, M. Leunig, S. K. Huang, D. A. Berk, D. Papahadjopoulos, and R. K. Jain. Microvascular permeability and interstitial penetration of sterically stabilized (Stealth) liposomes in a human tumor xenograft. *Cancer Res.* **54**:3352–3356 (1994).
10. R. K. Jain. Delivery of molecular and cellular medicine to solid tumors. *Adv. Drug Deliv. Rev.* **26**:71–90 (1997).
11. N. Z. Wu, D. Da, T. L. Rudoll, D. Needham, A. R. Whorton, and M. W. Dewhirst. Increased microvascular permeability contributes to preferential accumulation of stealth liposomes in tumor tissue. *Cancer Res.* **53**:3765–3770 (1993).
12. S. C. Kim, D. W. Kim, Y. H. Shim, J. S. Bang, H. S. Oh, S. W. Kim, and M. H. Seo. *In vivo* evaluation of polymeric micellar paclitaxel formulation: toxicity and efficacy. *J. Control. Release* **72**:191–202 (2001).
13. D. Le Garrec, S. Gori, L. Luo, D. Lessard, D. C. Smith, M. A. Yessine, M. Ranger, and J. C. Leroux. Poly(*N*-vinylpyrrolidone)-block-poly(D,L-lactide) as a new polymeric solubilizer for hydrophobic anticancer drugs: *in vitro* and *in vivo* evaluation. *J. Control. Release* **99**:83–101 (2004).
14. T. Y. Kim, D. W. Kim, J. Y. Chung, S. G. Shin, S. C. Kim, D. S. Heo, N. K. Kim, and Y. J. Bang. Phase I and pharmacokinetic stidy of Genexol-PM, a Cremophor free, polymeric micelle-formulated paclitaxel, in patients with advanced malignancies. *Clin. Cancer Res.* **10**:3708–3716 (2004).
15. A. Sharma, E. Mayhew, L. Bolcsak, C. Cavanaugh, P. Harmon, A. S. Janoff, and J. Bernacki. Activity of paclitaxel liposome formulations against human ovarian tumor xenograft. *Int. J. Cancer* **71**:103–107 (1997).
16. P. P. Constantinides, A. Tustian, and D. R. Kessler. Tocol emulsions for drug solubilization and parenteral delivery. *Adv. Drug Deliv. Rev.* **56**:1243–1255 (2004).
17. B. T. Hill, R. D. H. Whelan, S. A. Shellard, S. McClean, and L. K. Hosking. Differential cytotoxic effects of docetaxel in a range of mammalian tumor cell lines and certain drug resistant sublines *in vitro*. *Invest. New Drugs* **12**:169–182 (1994).
18. M. C. Bissery, D. Guénard, F. Guéritte-Voegelein, and F. Lavelle. Experimental antitumor activity of Taxotere (RP 56976, NSC 628503), a Taxol analogue. *Cancer Res.* **5**:4845–4852 (1991).
19. A. J. Ten Tije, J. Verweij, W. J. Loos, and A. Sparreboom. Pharmacological effects of formulation vehicles—implications for cancer chemotherapy. *Clin. Pharmacokinet.* **42**:665–685 (2003).
20. D. Le Garrec, M. Ranger, and J. C. Leroux. Micelles in anticancer drug delivery. *Am. J. Drug Deliv.* **2**:15–42 (2004).
21. J. Szebeni. Complement activation-related pseudoallergy caused by liposomes, micellar carriers of intravenous drugs and radiocontrast agents. *Crit. Rev. Ther. Drug Carrier Syst.* **18**:567–606 (2001).
22. N. Kang, M. E. Perron, R. E. Prud'Homme, Y. Zhang, G. Gaucher, and J. C. Leroux. Stereocomplex block copolymer micelles: core–shell structures with enhanced stability. *Nano Lett.* **5**:315–319 (2005).
23. X. Zhang, H. M. Burt, G. Mangold, D. Dexter, D. Von Hoff, L. Mayer, and W. L. Hunter. Anti-tumor efficacy and biodistribution of intravenous polymeric micellar paclitaxel. *Anti-Cancer Drugs* **8**:686–701 (1997).
24. X. Shuai, T. Merdan, A. K. Schaper, F. Xi, and T. Kissel. Core-cross-linked polymeric micelles as paclitaxel carriers. *Bioconjug. Chem.* **15**:441–448 (2004).
25. J. L. Liu and C. Allen. Polymer–drug compatibility: a guide to the development of delivery systems for the anticancer agent, ellipticine. *J. Pharm. Sci.* **93**:132–143 (2004).
26. T. Hamaguchi, Y. Matsumara, M. Suzuki, K. Shimizu, R. Goda, I. Nakamura, I. Nakatomi, M. Yokoyama, K. Kataoka, and T. Kakizoe. NK105, a paclitaxel-incorporating micellar nanoparticle formulation can extend *in vivo* antitumor activity and reduce the neurotoxicity of paclitaxel. *Br. J. Cancer* **92**: 1240–1246 (2005).
27. N. K. Ibrahim, N. Desai, S. Legha, P. Soon-Shiong, R. L. Theriault, E. Rivera, B. Esmaeli, S. E. Ring, A. Bedikian, G. N. Hortobayi, and J. A. Ellerhost. Phase I and pharmacokinetic study of ABI-007, a cremophor-free protein stabilized, nanoparticle formulation of paclitaxel. *Clin. Cancer Res.* **8**:1038–1044 (2002).
28. J. W. Singer, B. Baker, P. De Vries, A. Kumar, S. Shaffer, E. Vawter, M. Bolton and P. Garzone. Poly-(l)-glutamic acid-paclitaxel (CT-2103) [XYOTAX], a biodegradable polymeric drug conjugate: characterization, preclinical pharmacology, and preliminary clinical data. In H. Maeda, A. Kabanov, K. Kataoka, and T. Okano, (eds.), *Polymer Drugs in the Clinical Stage* (H. Maeda, A. Kabanov, K. Kataoka, and T. Okano, eds.), Kluwer Academic/Plenum Publishers, New York, 2003, pp. 81–99.
29. D. Hoarau, P. Delmas, S. David, E. Roux, and J. C. Leroux. Novel long-circulating lipid nanocapsules. *Pharm. Res.* **21**: 1783–1789 (2004).
30. B. Heurtault, P. Saulnier, B. Pech, J. E. Proust, and J. P. Benoit. A novel phase inversion-based process for the preparation of lipid nanocarriers. *Pharm. Res.* **19**:875–880 (2002).
31. P. S. Uster, T. M. Allen, B. E. Daniel, C. J. Mendez, M. S. Newman, and G. Z. Zhu. Insertion of poly(ethylene glycol) derivatized phospholipid into pre-formed liposomes results in prolonged *in vivo* circulation time. *FEBS Lett.* **386**:243–246 (1996).
32. M. Ramaswamy, X. Zhang, H. M. Burt, and K. M. Wasan. Human plasma distribution of free paclitaxel and paclitaxel associated with diblock copolymers. *J. Pharm. Sci.* **86**:460–464 (1997).
33. J. A. MacKay, D. F. Deen, and F. C. Szoka Jr. Distribution in brain of liposomes after convection enhanced delivery; modulation by particle charge, particle diameter, and presence of steric coating. *Brain Res.* **1035**:139–153 (2005).
34. T. L. Andresen, S. S. Jensen, and K. Jorgensen. Advanced strategies in liposomal cancer therapy: problems and prospects of active and tumor specific disease. *Prog. Lipid Res.* **44**:68–97 (2005).
35. V. S. Trubetskoy and V. P. Torchilin. Use of polyethylene–lipid conjugates as long-circulating carriers for delivery of therapeutic and diagnostic agents. *Adv. Drug Deliv. Rev.* **16**:311–320 (1995).